Materials Research Express

PAPER • **OPEN ACCESS**

Li and Na-ion diffusion and intercalation characteristics in vertically aligned TiS_2 nanowall network grown using atomic layer deposition

Materials Research Express

PAPER

Li and Na-ion diffusion and intercalation characteristics in vertically aligned TiS_2 nanowall network grown using atomic layer deposition

Farheen N Sayed[1,3,4], **M B Sreedhara**[2,3,5], **Amit Soni**[2], **Usha Bhat**[2], **Ranjan Datta**[2], **Aninda J Bhattacharyya**[1,6] and **C N R Rao**[2,6]

[1] Solid State and Structural Chemistry Unit, Indian Institute of Science, Bengaluru-560012, India
[2] School of Advanced Materials (SAMat) and Sheikh Saqr Laboratory, Jawaharlal Nehru Centre for Advanced Scientific Research, Jakkur PO, Bengaluru-560064, India
[3] FNS and MBS have contributed equally to this work.
[4] Presently at University of Cambridge, United Kingdom.
[5] Presently at Weizmann Institute of Science, Rehovot, Israel.
[6] Authors to whom any correspondence should be addressed.

E-mail: anindajb@iisc.ac.in **and** cnrrao@jncasr.ac.in

Keywords: Li/Na ion diffusion, intercalation chemistry, TiS_2, atomic layer deposition (ALD), rechargeable batteries

OPEN ACCESS

RECEIVED
23 June 2019

REVISED
8 August 2019

ACCEPTED FOR PUBLICATION
23 August 2019

PUBLISHED
1 November 2019

Abstract

We present here the study of diffusion and intercalation mechanisms of Li-ion and Na-ion in titanium disulfide (TiS_2) films grown by atomic layer deposition (ALD). The layered TiS_2 has been explored here due to the interesting differences between the intercalation mechanisms of Li^+ and Na^+. The ALD grown TiS_2 films further facilitate the study as this method provides compact and dense films with no polymer binder and carbon additives. The diffusion and intercalation processes are observed to depend on the ionic size and character of the solid electrolyte interphase. The increased capacity obtained for the present ALD synthesized samples is attributed to the enhanced anchoring ability of the TiS_2 films, which comprises of an extended nanowall network. The charge transfer resistance (R_{ct}) obtained from impedance data correlate well with the lithiation steps observed in the galvanostatic discharge-charge studies. At potentials where lithiation takes place, R_{ct} value is observed to drop. This direct correlation is however, not observed between the R_{ct} and sodiation potential. The diffusion coefficients, calculated using GITT and impedance methods, are observed to be independent of the type of Li-salts. However, the variation of diffusion coefficients with the lithiation/sodiation voltages are different. This is attributed to the combined differences in the ionic radii and phase formation. Intercalation-de-intercalation in to TiS_2 coated with alumina is also studied here. Coating with alumina results in a stable SEI. However, coating leads to higher R_{ct}, lower D_{Li+} and poor capacity retention as a function of cycle number.

1. Introduction

Intercalating host materials based on carbon (e.g. graphite), transition metal layered oxides and dichalcogenides have been widely used as electrodes in alkali-ion rechargeable batteries especially the Li-ion batteries [1–3]. Many of the intercalation materials whether oxides or sulfides, consist of a close-packed anion sublattice comprising of an array of octahedral and tetrahedral interstitial sites for occupation by the transition metal ions. On intercalation, the possibility of occupation of either an octahedral or a tetrahedra site by an alkali-ion is governed by the alkali-ion size and factors related to the intrinsic host crystal structure viz. space availability at the intercalation site, chemical characteristics of the site, and mechanical stability of the lattice following intercalation [4]. In addition to these matters, the inherent crystal structure of the host provides a complex diffusion barrier landscape which imposes a strong concentration dependent alkali-ion diffusion behavior. For cathode intercalation materials such as $LiCoO_2$ and $LiNi_{1/3}Mn_{1/3}Co_{1/3}O$ the lithiation plateau is a signature of the transition from Li-deficient to Li-rich phase and may involve order-disorder transitions, two phase reaction and structural phase transitions [5]. In case of layered anode TiS_2 electrochemical intercalation of Li^+-ion

proceeds via the formation of a homogenous solid solution. The intercalation of Li and other alkali ions, as Na, Mg, Ca and K, in TiS_2 can be strongly affected by the concentration and extent of ordering of these alkali ions in layer [6–9].

TiS_2 crystallizes in a hexagonal close packed (hcp) structure similar to that of CdI_2. In TiS_2, half of the octahedral sites are filled with Ti^{4+} which in turn is surrounded by six sulfide anions in an octahedral environment. The layers of TiS_2 thus formed, consist of covalent Ti–S bonds and individual layers of TiS_2 are bound together by van der Waals forces [10]. Since the pioneering work by Whittingham [11] and it's demonstration as an electrode in rechargeable batteries [12], considerable focus has been on the study of the ion diffusion mechanism of different alkali-ions in TiS_2. It has been proposed that diffusion in TiS_2 (3D) crystal structure is often mediated by vacancy clusters such as di-vacancies due to it's lower migration barrier for Li^+-ions compared to that for isolated vacancies [5]. Moving from Li^+-ion, transfer barriers for Na^+/K^+-ions in TiS_2 are significantly higher mainly due to their larger ionic radius of (Na^+-ion $\approx$ 1.86 Å; K^+-ion $\approx$ 2.31 Å) as compared to Li^+-ion ($\approx$ 1.52 Å). The intercalation and hence, structural chemistry of other alkali ions (Na^+, K^+) and alkaline ions (Mg^+) are more complex as these ions can occupy either octahedral and trigonal prismatic sites [6, 13, 14]. For any metal-ion intercalation in a layered structure, as the transfer of electrons from the intercalated ion to the host TiS_2 lattice occurs, the relatively weaker van der Waals forces are replaced by stronger coulombic interactions among the layers. For the investigation of alkali metal intercalation, thin films provide better scope than the conventional thicker electrode cast on a current collector with binder and conducting carbon. TiS_2 thin films has been grown using various methods like Activated Reactive Evaporation process, Chemical Vapour Deposition (CVD) and Pulsed Laser Deposition (PLD) [15–18]. In this work, to study the transport and storage properties of TiS_2 thin films were grown using atomic layer deposition (ALD). ALD is employed here as it provides great opportunities to systematically control the materials microstructure leading to high quality thin films tailormade for task specific applications [19, 20].

We present here the study of Li^+ and Na^+ -ion diffusion characteristics in TiS_2 and alumina coated TiS_2 electrode grown via ALD method. The ALD method allows highly uniform and direct deposition of a TiS_2 film on to the current collector. This nullifies the usage and influence of polymer binder and carbon additive which typically arises from the conventional solution-based casting procedures. Galvanometric intermittent titration (GITT) and ac-impedance methods have been employed to compare the distinctive diffusion mechanisms of Li^+ -ions and Na^+ -ions in bare as well as alumina coated TiS_2 and it's eventual impact on the intercalation process in the samples.

2. Experimental

2.1. Deposition of TiS_2 thin films using atomic layer deposition

TiS_2 thin films having nanowall network morphology are grown by atomic layer deposition on single crystalline c-sapphire (0001), and stainless steel using a flow type Beneq TFS 200 ALD reactor (Finland Oy). Titanium tetrachloride ($TiCl_4$, 99.9%, Alfa Aesar) and hydrogen sulfide (H_2S, Bhuruka gases, 97.5%) are employed as Ti and S precursors respectively. Highly pure nitrogen, N_2 (Chemix, 99.9995) is used as a process and purging gas throughout the deposition. The reactor and chamber of the ALD system are evacuated to a minimum pressure of 1 and 10 mbar before starting the deposition. The reactor and chamber are heated to 300 °C and allowed to stay for 30 min to stabilize the temperature. $TiCl_4$ precursor is kept in a liquid bubbler and maintained at 20 °C. The precursor is allowed to enter the reactor by it's own vapor pressure without any booster step. The TiS_2 film is deposited by consecutive pulsing of $TiCl_4$ and H_2S. The chamber pressure is almost constant during the deposition whereas variation in the reactor pressure between 1–3 mbar is observed during pulsing and purging of the precursor. To ascertain self-terminating nature of ALD process and ALD temperature window, the depositions are carried out at different reactor temperatures and pulse and purge times. The temperature window for the ALD growth is tested between 150 and 300 °C. The films appear to grow more uniformly at 300 °C without any residual chlorine. The pulse and purge times for $TiCl_4$ are respectively 400 ms and 3 s, whereas the pulse and purge times for H_2S are respectively 1 s and 3 s. The complete one cycle sequence of ALD for TiS_2 growth is pulse $TiCl_4$ (200 ms)/purge (3 s)//pulse H_2S (1 s)/purge (3 s). The deposition is carried out for 500, 1000, 1500 and 2000 cycles at 300 °C. The films are cooled down slowly to room temperature in vacuum under continuous flow of N_2. The as-obtained films appear to be black in color and used as it is for detailed characterization without any further temperature treatement.

2.2. Deposition of Al_2O_3 on TiS_2 thin film

A thin layer of Al_2O_3 of 5–6 nm is deposited using thermal ALD process by employing trimethylaluminum (TMA) and water as Al and O precursor respectively. An optimised recipe of Al_2O_3 with the growth rate of

0.12 nm per cycle is employed for this purpose. The reactor temperature is maintained at 200 °C during the growth and is repeated for 50 ALD cycles.

2.3. Structural characterization of TiS_2 thin films

X-ray diffraction (XRD) patterns of the as-deposited films on c-sapphire (0001) are recorded with a Panalytical Empyrean diffractometer (Cu $K\alpha_1$ radiation; $\lambda = 1.5404$ Å). Thickness and surface morphology of the films are studied using field emission scanning electron microscope (Nova NanoSEM 600 FESEM) equipped with an energy dispersive x-ray (EDX). Raman spectra are recorded using a Jobin Yvon LabRam HR spectrometer in backscattering geometry using a 514 nm Ar laser. X-ray photoelectron spectra (XPS) are obtained using an Omicron nanotechnology spectrometer with Mg-Kα x-ray source. Estimation of cross-section of samples from transmission electron microscopy is prepared in two steps. Initially, sample is thinned down to a few micrometers by mechanical polishing and then perforation is done using ion milling using Argon (Ar) gas. This perforation provides a thin layer (few nm thickness), which is electronically transparent for transmission electron microscopy. Polishing is done carefully so that the weak van der Waals layers of TiS_2 do not delaminate from the substrate. Cross-sectional high-resolution TEM (HRTEM) images are obtained from double aberration corrected FEI TITAN 80–300 kV microscope at 300 kV.

2.4. Electrochemical characterization

All the electrochemical measurements are performed in a coin cell configuration of TiS_2 electrode deposited on stainless steel spacer disk. The pure metals (Li and Na) are used as both reference and counter electrodes separated by electrolyte-soaked quartz separator. The three electrolytes used in present study are prepared by dissolving 1 M salts of $LiPF_6$, $LiClO_4$ and $NaClO_4$ in equimolar (1:1) ethyl carbonate and dimethyl carbonate solutions. The cyclic voltammogram (CV) are recorded in a potential window 0.5–3.0 V with 0.01 mV s^{-1} on CH instrument (CH403). Galvanostatic charge-discharge cycling is also performed in the same potential window at a specified current rate. All galvanostatic measurements including GITT studies are performed using Arbin Instrument. Electrochemical impedance spectra (EIS) are recorded in the frequency range of 0.01 Hz to 1 MHz with amplitude of 0.001 V on a CH instrument.

2.5. Diffusion coefficient from GITT method

The coin cells are pre-stabilized by running it through four successive discharge-charge cycles. The procedure for GITT is adopted [21] and has been suitably modified for layered and 3D materials' diffusion studies [22–24]. For GITT study, the cell following stabilization is discharged (from 3.0 V) for 30 min at constant current and then allowed to be under open circuit condition for 2 h, followed by again discharging for 30 min and 2 h of rest time till it reaches the minimum of potential window i.e. 0.5 V. The equation for estimating the diffusion coefficient is as follows:

$$D_{Li} = \frac{4}{\pi\tau}\left(\frac{mV_M}{MS}\right)^2\left(\frac{\Delta E_s}{\Delta E_t}\right)^2, \ \tau \ll L^2/D_A$$

where, m is the mass of the active electrode material, V_M and M are the molar volume and molar mass of TiS_2 respectively, S is the electrode-electrolyte geometrical contact area, τ is the constant current pulse time, and ΔE_s and ΔE_t are respectively the changes in the equilibrium potential and potential during hold time.

2.6. Diffusion coefficient from Warburg impedance

The method, first proposed by Ho *et al* [25], has been utilized widely in the recent years with the aim of monitoring the diffusion coefficient at each stage of lithiation/sodiation [26]. The equation for Warburg impedance and relation for estimation of the diffusion coefficient are as follow:

$$-Z_{Im} = \delta\omega^{-1/2}$$
$$\delta = \frac{V_m}{zFAm(2D)^{1/2}}\left(\frac{dE_{oc}}{dx}\right), \ \omega \gg D/R^2$$

where, ω is the angular frequency, δ is the Warburg pre-factor, V_m is the molar volume of lithiated material, (dE_{oc}/dx) is the gradient of the coulometric titration curve, which is obtained from a plot of the open-circuit potential versus the composition 'x' at each charged state, m is the amount of active material in the electrode, z is the charge number of the electroactive species, here 1 for both Li^+ and Na^+ -ion.

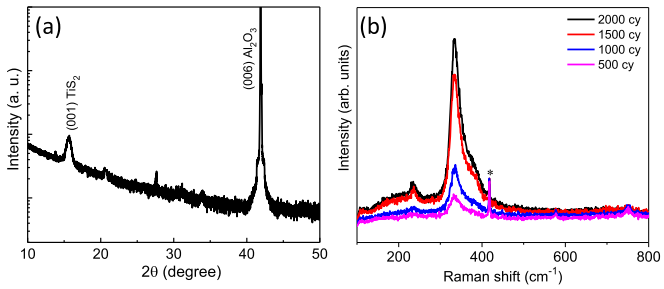

Figure 1. (a) X-ray diffraction pattern and (b) Raman spectrum of as grown TiS_2 thin films on *c*-sapphire substrate.

3. Results and discussion

3.1. Phase and morphology

TiS_2 thin films having nanowall network morphology are grown on various substrates including *c*-sapphire and stainless steel using thermal ALD process by pulsing $TiCl_4$ and H_2S precursors. The ALD temperature regime and other process parameters are optimized to achieve self-limiting surface saturation reaction with large area uniform films. Due to a network-type of morphology, it is difficult to precisely determine the thickness of the film. To avoid back etching reactions resulting from by-products, the purge time is kept long enough. We observe uniform growth with the same morphology at 300 °C, even with a higher pulse duration of $TiCl_4$ and H_2S without any chlorine contamination. The crystalline films on *c*-sapphire are obtained at a reactor temperature of 300 °C. All other depositions for further studies are carried out at 300 °C, with pulsing and purging times of 2 s and 4 s for $TiCl_4$ and H_2S respectively.

The phase diagram of Ti-S includes many stoichiometric ratios, the stable form being TiS_2. Under certain conditions, TiS_2 may convert to TiS via an intermediate phase, Ti_2S_3. Among these phases, the TiS_2 structure is the favored phases from the point of view of intercalation [27]. Excess of titanium can cause pinning of the sulfide layers which will reduce the diffusion of the alkali ions and at the same time occupy some of the sites where the Li^+ ion would otherwise reside [11]. The TiS_2 films are analyzed using x-ray diffraction without any post temperature treatment. Figure 1(a) shows x-ray diffraction pattern of TiS_2 film grown at 300 °C for 2000 cycles. The reflections reveal lines corresponding to TiS_2 and *c*-sapphire substrate. The films are crystalline in nature and reflections can be indexed to (001) of TiS_2 ($2\theta = 15.6°$) along with (006) of *c*-sapphire ($2\theta = 41.8°$). The appearance of (00l) reflections in the diffraction pattern suggests that ordered growth of TiS_2 on *c*-sapphire. The appearance of broader and weaker reflections of TiS_2 indicate that there may be also amorphous regions present in the film along with the crystalline regimes which can be attributed to the lower deposition temperature. Additionally, the thickness of the films is in the nanometers range and vertical network morphology might also affect the intensity and width of the reflections. From XRD studies, the crystal geometry relation between the substrate and film is found to be $\langle 0001 \rangle$ TiS_2//$\langle 0001 \rangle$ Al_2O_3 (*c*-sapphire). The crystallinity on *c*-sapphire may arise due to the same hexagonal crystal geometry with less lattice mismatch. The films grown on substrates such as Si(100), stainless steel and quartz are amorphous. Hence, the characterization here after is preferably done on c-sapphire. We investigated the optical properties of TiS_2 films of various thickness under ambient conditions using Raman spectroscopy (laser excitation wavelength 514 nm). The Raman spectra in figure 1(b) show significant phonon scattering signals at 235 cm^{-1} due to the in-plane E^1_{2g} mode and 336 cm^{-1} the out-of-plane A_{1g} optical phonon modes of TiS_2. Prominent A_{1g} mode suggests that a strong covalent bond exists between the intra-layer atoms and van der Waals force between the layers [28]. The x-ray photoelectron spectrum shows characteristic signal due to Ti(2p) and S(2p) corresponding to TiS_2 bonding (figure S1). The atomic composition calculated from the XP spectra is found to be $Ti_{0.32}S_{0.68}$ and the composition is almost similar irrespective of the underlying substrate.

Surface morphology of TiS_2 films are studied by FE-SEM. Figures 2(a–d) show the in-plane view images of TiS_2 film grown for 2000 ALD cycles on the *c*-sapphire substrate. The FE-SEM images reveal clearly the nanowall network morphology of the TiS_2 films. Images acquired at high-resolution reveal that each individual nanowall structure comprise of several van der Waal layers of TiS_2. The 2D sheets grow vertically and combine with the edges of adjoining nanosheets making an expansive nanowall network. The growth of the individual nanowall is regular and uniform throughout and the thickness of the each nanowall is nearly the same in the network.

The network shows the presence of pores or voids in between the nanowalls. The network morphology is similar irrespective of the underlying substrates (figure S2). The minor differences such as wider wall thickness and different pore sizes may be due to slight variations in the growth rate and differences in surface roughness

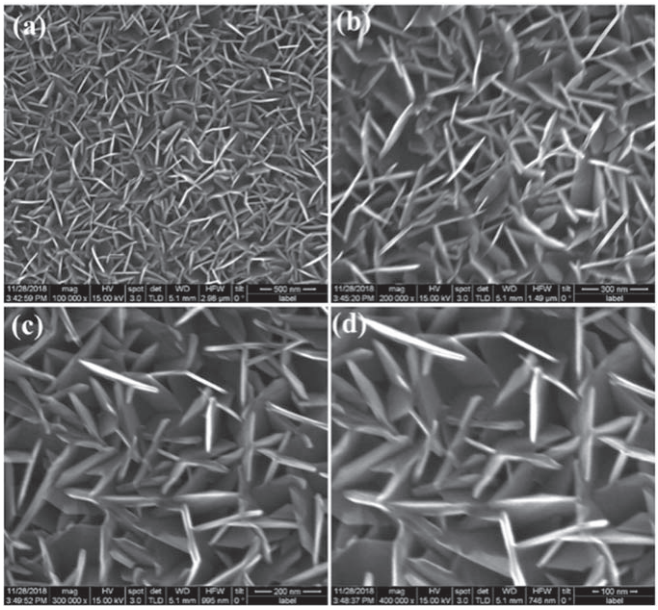

Figure 2. (a)–(d) Plane-view FESEM images showing the surface morphology of the as-deposited 2000 ALD cycle grown crystalline TiS_2 thin films on the *c*-sapphire substrate.

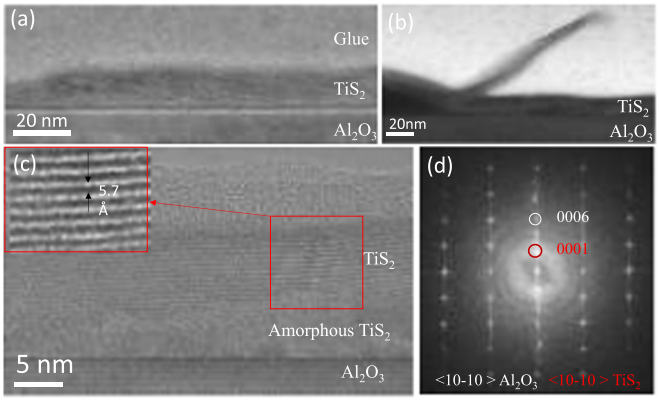

Figure 3. (a) Cross sectional bright field TEM image of TiS_2 thin film grown on *c*-sapphire and (b) growth of TiS_2 thin film away from the film-substrate interface. (c) High-resolution TEM image of TiS_2 thin film, interlayer distance is 5.7 Å and is marked in the inset and (d) corresponding FFT pattern both from film and substrate. The epitaxial relationship is $\langle 0001 \rangle$ Al_2O_3 || $\langle 0001 \rangle$ TiS_2 and $\langle 10\text{–}10 \rangle$ Al_2O_3 || $\langle 10\text{–}10 \rangle$ TiS_2.

between the *c*-sapphire and stainless steel substrates. The stainless steel is polycrystalline and rougher compared to the single crystalline c-sapphire.

Cross-section TEM is used to comprehend the crystalline growth pattern of the TiS_2 films on the *c*-sapphire substrate. Prior to TEM characterization, the films are mechanically polished for acquiring higher quality images. Low magnification TEM image in figure 3(a) confirms the layered growth of TiS_2 film on *c*-sapphire. At many places, film is observed to grow away from the film-substrate interface, creating a network-like structure of varying thickness 5 to 20 nm which can be seen in figure 3(b). High-resolution transmission electron microscope (HRTEM) images show that the TiS_2 is polycrystalline or amorphous on the substrate, approximately up to 5 to 10 nm and then the van der Waals layers are formed above that (figure 3(c)). The number of layers vary from place to place, approximately 10 to 15 layers with the interlayer distance of 5.7 Å. Figure 3(d) corresponds to the fast Fourier transform (FFT) of substrate, interface and layers together. The epitaxial relationship is $\langle 0001 \rangle$ TiS_2 || $\langle 0001 \rangle$ Al_2O_3 and $\langle 10\text{–}10 \rangle$ TiS_2 || $\langle 10\text{–}10 \rangle$ Al_2O_3. In figure S3(a), we clearly see vertical growth of TiS_2 network away from the substrate interface which is consisted with FESEM studies. Figure S3(b) shows polycrystalline regions of TiS_2 from the substrate surface. Figure S4 depicts the FFTs patterns generated from the different regions of figure S3(b).

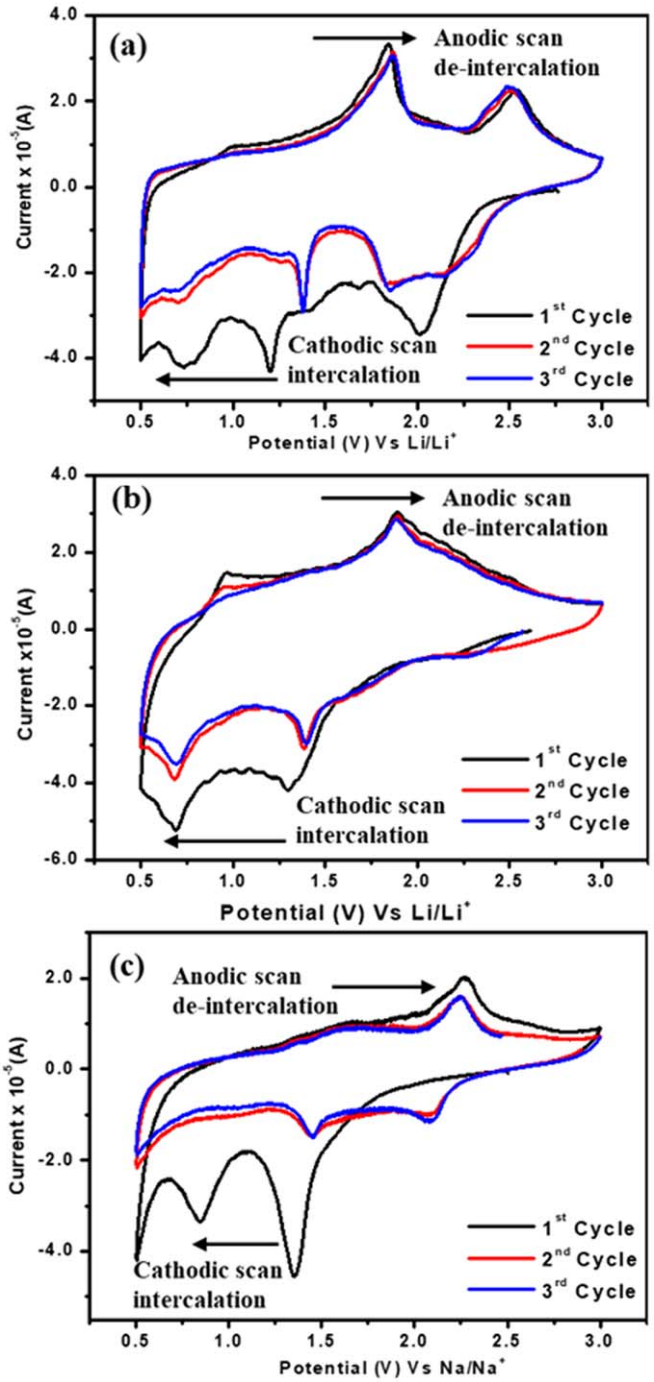

Figure 4. Cyclic voltammogram depicting intercalation-deintercalation behavior of Li-ion in the electrochemical potential window (0.5–3.0) V with a scan rate 0.01 mV s^{-1} using 1 M Li ion salts (a) $LiPF_6$ and (b) $LiClO_4$ in EC:DMC. (c) Intercalation-deintercalation behavior of Na-ion in TiS_2 (potential window: (0.5–3.0) V; scan rate: 0.01 mV s^{-1}) electrode using 1 M $NaClO_4$ in EC:DMC. In (a) and (b) the Li-foil is the anode whereas in (c) Na metal foil is the anode. (The first step in all the CVs is cathodic scan).

3.2. Li^+ and Na^+ intercalation-deintercalation in TiS_2

Figure 4 depicts the cyclic voltammograms with regard to Li-ion and Na-ion intercalation and deintercalation in TiS_2. The voltammograms show signatures corresponding to the formation of a full range of solid solutions of Li_xTiS_2 ($0 < x < 1$) due to the lithiation and delithiation. The potential window of (0.5–3.0) V is selected to avoid the conversion reaction: $LiTiS_2 + 3Li^+ + 3e^- \rightarrow 2Li_2S + Ti$ which is supposed to be dominant process at voltages lower than 0.5 V [29]. Figure 4(a) for $LiPF_6$ in EC:DMC depicts a complex and multi-step lithiation process are observed. Four prominent lithiation peaks at 2.01, 1.41, 1.20 and 0.73 V are observed, whereas only two de-lithiation peaks are observed at 1.85 and 2.53 V.

However, a different Li-ion intercalation behavior is observed with $LiClO_4$ salt (figure 4(b)). Two distinct lithiation peaks at 1.30 and 0.69 V and de-lithiation peaks at 1.88 and 0.95 V are observed in the 1st cycle. In the

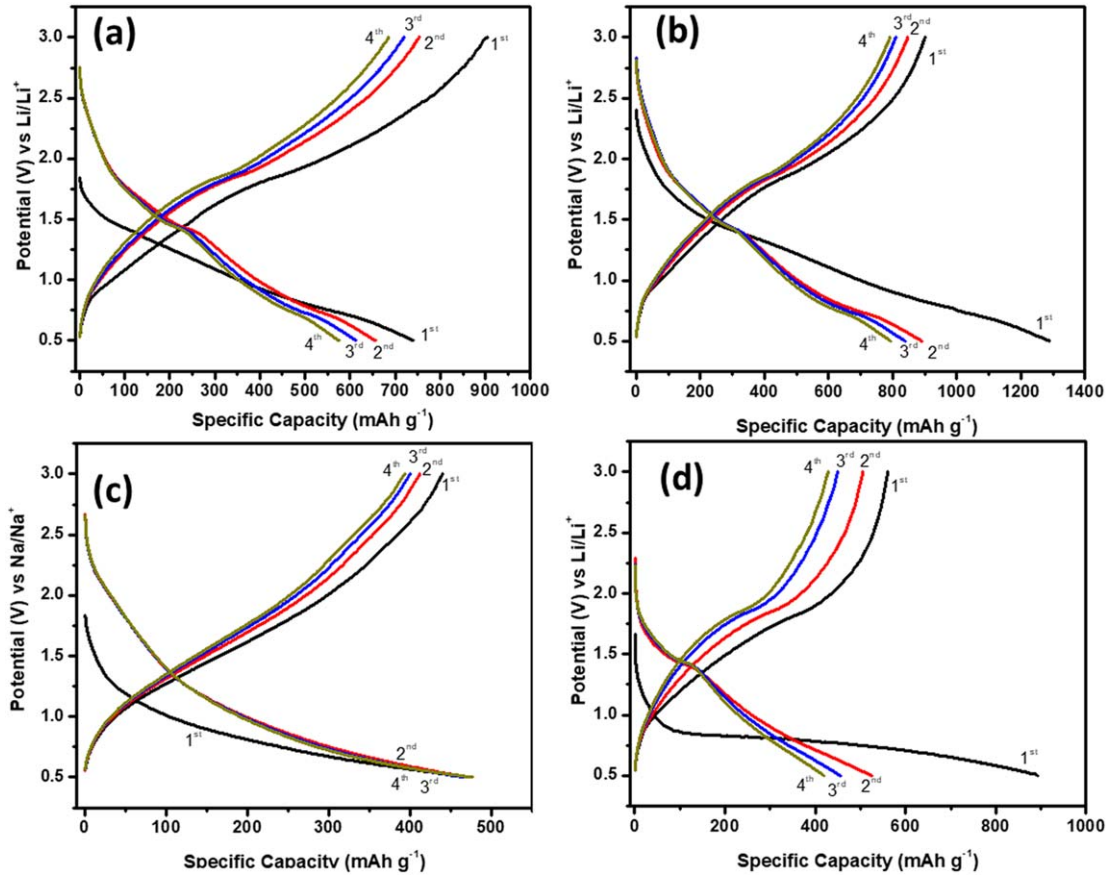

Figure 5. Galvanostatic discharge-charge profiles for TiS_2 with (a) 1 M $LiPF_6$ versus Li metal, (b) 1 M $LiClO_4$ versus Li metal, (c) 1 M $NaClO_4$ versus Na metal and (d) alumina-coated TiS_2 with $LiPF_6$ versus Li metal with 100 mA g^{-1} current density in potential range of (0.5–3.0) V starting with cathodic scan first.

subsequent cycles, the intensity of the lithiation peaks decreases to a greater extent than the delithiation peaks. The magnitude of peak current however, in the two Li-salts are nearly the same. For Na^+-ion intercalation, employing $NaClO_4$ in 1:1 EC:DMC the cathodic peaks are observed to be same as in case of $LiPF_6$ in EC:DMC. Here, the high voltage peak at 2.07 V appear from the second cycle onwards (figure 4(c)).

The corresponding anodic peak at 2.27 V is clearly visible from the First cycle itself. The intercalation mechanism of Li^+ and Na^+ -ions, irrespective of salt and solvent selection, is attributed to the relatively weakly binding interlayer forces as well as the amenability of the Ti^{4+} centers to reduce to Ti^{3+}. Published reports of Na^+-ion intercalation in to TiS_2 suggests the appearance of two prominent peaks positioned at 2.07 and 1.35 V. Consistency of the observations reported here with published reports suggests the formation of two different phases upon Na^+ -ion insertion: Na_xTiS_2, (where $x = 0 < x < 0.4$) and Na_yTiS_2 ($y = 0.4 < y < 0.8$) [11]. The Na^+-ion intercalation also involves prismatic co-ordination which eventually results into two distinct regions assigned to Na^+ -ion intercalation.

Interestingly the subsequent cycles show stable behaviour with no trace of the 0.84 V sodiation peak. Formation of a homogenous solid solution with intercalating ions is typically reflected via the observation of a smooth sloping voltage plateau in the discharge/charge profile. In present study, sloping voltage plateau is observed with the Li^+ and Na^+ -ion intercalation/de-intercalation phenomenon in TiS_2, figure 5(a–d). In the first cycle additionally, a small flat plateau region is observed. In non-layered materials, this has been assigned to 1^{st} order phase transition. However, in present case of layered TiS_2, where formation of solid solutions is predominant [7], the presence of plateau region around 0.7 V in discharge step is due to the formation of a stable solid electrolyte interphase (SEI) at the electrode surface, which remains intact in the subsequent cycles. The plateau is observed to be more prominent in the first cycle for the alumina coated TiS_2 sample with the $LiPF_6$ based electrolyte (figure 5(d)). This suggests that SEI formation is more feasible in the presence of alumina coating. Additionally it allows breathing space in the intrinsic structure following the intercalation of ions. Also, huge irreversible capacity (≈ 375 mAh g^{-1}) is obtained in alumina coated sample in first discharge step. With regard to the Na^+-ion

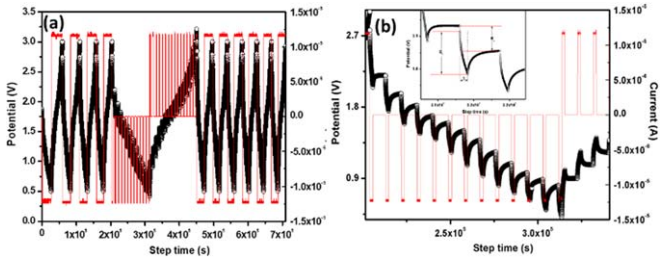

Figure 6. (a) Galvanostatic discharge—charge cycles followed by GITT experiment where the TiS_2 with $LiPF_6$ in EC:DMC electrolyte cell is intermittently charged versus Li following resting in the open circuit condition for 2 h. (b) Enlarged figure focusing on GITT experiment in cathodic step and inset show the parameters used to calculate the diffusion coefficient.

intercalation, irreversible loss in capacity is much less compared to the Li^+ counterparts. This suggests that the presumed SEI formation for a Na^+-ion-based system is less compared to that for Li^+ -ion based system.

For all the above, the 1st cycle specific capacity obtained are much higher than the reported values. In our earlier studies on MoS_2 samples prepared by the same ALD technique, capacity higher than the theoretical values were reported [29]. This was attributed to the activation of more number of surface adsorption sites which results in a higher degree reversible intercalation with the alkali-ion leading to higher charge/energy storage. In the present study, we have also restricted the lower potential limit to 0.5 V so as to completely eliminate the contributions from conversion reaction of electrode. With $LiPF_6$ based electrolyte (figure 5(a)), the first cycle charge capacity is more suggesting increased oxidation of electrolyte at the TiS_2 surface and hence SEI formation at the TiS_2 electrode will be feasible. For $LiClO_4$ based electrolyte, the first cycle discharge capacity is the highest. However, a higher irreversible capacity loss is observed which can be assigned to the higher salt decomposition and probably a thicker SEI.

The discharge - charge cycling behavior at different current values has also been performed. It is observed that the efficiency of discharge—charge cycles at slower current rate is less as compared to the high current rate values (figure S5). The cells, however, could not be run at higher current values due to the fact that the thin films employed here have very less active materials, in micrograms range. On decreasing back to the initial lower current values, the capacity values measured earlier could be retraced back.

Following the studies related to the intercalation-deintercalation of Li^+ and Na^+-ions in TiS_2 host lattice, we now turn our attention to the study of intercalation mechanism and diffusion kinetics in TiS_2. As discussed in the introduction, two methods have been adopted to calculate the diffusion coefficient of Li^+ and Na^+-ions in TiS_2. These are detailed in the subsequent section.

3.3. Determination of the Li/Na ion diffusion coefficient by GITT method

The TiS_2 electrode in coin cell configuration is first equilibrated by carrying out four cycles of discharge and charge as shown in figure 6. The D_{Li+} values calculated from GITT method for TiS_2 in $LiPF_6$ based electrolyte is 2.14×10^{-13} cm^2 s^{-1}. Changing over from $LiPF_6$ to $LiClO_4$, the D_{Li+} remains the same strongly suggesting that the same electrochemical intercalation behavior of Li^+ even in the presence of different anions. In the case of the Na-salt, the D_{Na+} is estimated to be 2.01×10^{-13} cm^2 s^{-1}, which is almost same as D_{Li+}. However, the alumina coated sample show a drastic decrease in D_{Li+}, equal to 0.354×10^{-13} cm^2 s^{-1}. The alumina coating may contribute towards the stability in the charge and discharge states by forming stable SEI however, prevents further diffusion of the ions. The origin of this barrier results in extended SEI formation as observed in First discharge cycle in figure 5(d).

As witnessed by *insitu* and *exsitu* characterization techniques lithium intercalation is further complicated by ordering of lithium ion causing nonuniform lattice expansion in subsequent intercalation process [30]. Hence, we move towards the EIS method where diffusion behavior can be monitored at different intercalation-deintercalation potentials and will provide better insight.

3.4. Determination of the Li/Na ion diffusion coefficient by the EIS method using Warburg impedance

Electrochemical impedance spectra are recorded at different states of charge for TiS_2 in 1 M $LiPF_6$ based electrolyte is shown in figure 7(a). Prior to the recording of the impedance data, the samples are equilibrated at its open circuit potential value for 4 h. The charge transfer resistance (R_{ct}) calculated from the impedance data makes an interesting comparison with the lithiation plateau obtained in figure 5(a) (also in inset of figure 7(b)). On approaching the first lithiation plateau (=1.45 V), R_{ct} values drops to lower than that calculated at OCP. The R_{ct} value increases further with decrease in voltage till the next lithiation process at 0.81 V and drops again and with slight increase at the terminating cathodic potential (=0.5 V). It can be proposed that on approaching the

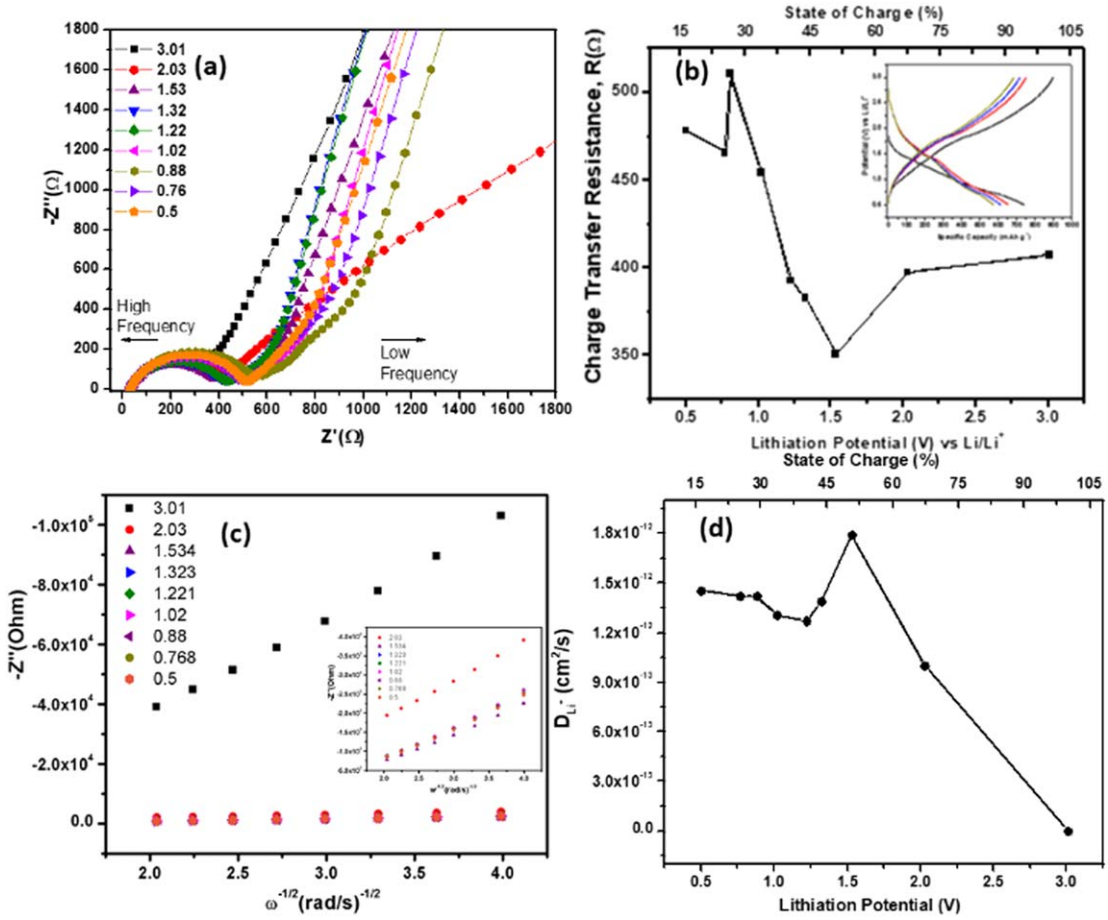

Figure 7. (a) Electrochemical impedance spectra of TiS_2 electrode in $LiPF_6$, EC:DMC electrolyte versus Li-metal as anode at different lithiation potentials. Prior to data collection, the cells are held for 1 h for completion of the lithiation process (b) Charge transfer resistance values (R_{ct}) calculated from impedance spectra (as in (a)) at different lithiation potential by monitoring the intercepts at real Z′ axis at lower frequency part of the semicircle, these lithiation potentials are in discharge steps (shown in inset) (c) Imaginary part of impedance data versus square root of the angular frequency and (d) diffusion coefficient values versus lithiation potential/state of charge.

lithiation potential, the impedance decreases suggesting higher ability of the host to accept Li^+ ions. This also infers the spontaneous nature of lithiation in TiS_2. Chemical lithiation is very facile for TiS_2 suggesting very small or no change in the stabilization energy of the non-lithiated and lithiated states leading to the solid solution formation. The impedance data shows a second semicircle in the low frequency regime for few of the equilibrated lithiation potentials (2.03, 0.88, 0.76 and 0.50 V). This suggests the simultaneous presence of lithiated and unlithiated phases leading to the formation of solid solution in successive potential steps. The range of EIS spectra in the lower frequency range where the lithiation is assumed to be diffusion controlled is used for the calculation of the diffusion coefficient. The Warburg impedance Z_w in the low frequency diffusion-controlled region is plotted as in figure 7(c) as a function of $\omega^{-1/2}$ at different state of charges (SOCs). The slope value is used to calculate the diffusion coefficient by employing the equation as described in experimental section.

The coulombic titration curve of potential versus x ($Ti_{1-x}S_2$, x = 0 to 1.0) is used to calculate the value of dE_{oc}/dx and for example is found to be 0.82 for $LiPF_6$ based electrolyte. The diffusion coefficient (D_{Li+}) calculated from this method lies in the range 9.50×10^{-16} to 1.45×10^{-12} $cm^2\ s^{-1}$ with the potential changing from 3.01 to 0.5 V. By similar calculation Na^+ intercalation in TiS_2 (with $NaClO_4$ in EC:DMC electrolyte) yielded a diffusion coefficient (D_{Na+}) range of 7.30×10^{-17} to 3.93×10^{-13} $cm^2\ s^{-1}$ in the voltage range from 1.91 to 0.56 V (corresponding plots are given in figure S6).

It is to be noted that at ≈1.5 V potential, where the R_{ct} value is minimum for Li^+ ion in $LiPF_6$ based electrolyte, the calculated D_{Li+} is highest, strongly suggesting the correlation of internal impedance with feasibility of Li^+ -ion diffusion in the layered structure. For Na^+ -ion diffusion however, D_{Na+} versus sodiation potential do not follow the same trend as the R_{ct} versus sodiation potential. As highlighted in the literature,

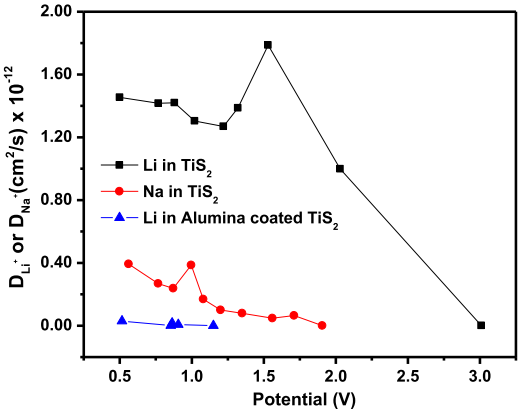

Figure 8. Comparative Li^+ and Na^+ -ion diffusion coefficients for bare TiS_2 and Li^+ -ion diffusion coefficient for alumina coated TiS_2 sample calculated from Warburg impedance values in lower frequency range of electrochemical impedance spectra.

structure and chemical composition of layered materials significantly affect the alkali metal-ion transport and intercalation behavior. It has been observed that heavier alkali metals prefer either an octahedral or trigonal prismatic lattice site unlike Li^+ which preferably occupy octahedral sites [6, 31]. In the case of Na^+-ion intercalation, sodiation in a controlled manner occurs only in alternate layers of TiS_2. Otherwise, random sodiation will lead to a two phase region [14]. At lower Na^+-ion concentrations trigonal prismatic lattice site is preferred whereas at higher Na^+ -ion concentration (and with decreasing sodiation potential) the more stable octahedral sites are occupied. In present study, both R_{ct} and D_{Na+} remains almost constant from 1.6 to 1.1 V. The R_{ct} value then suddenly increases at 1.0 V and then gradually increases from 0.9 to 0.5 V as in figure S6(b). On the other hand, the D_{Na+} slowly start to increase from 1.1 V till about 0.9 V. This behavior can be associated with the two-phase transition resulting from trigonal prismatic to octahedral site occupancy of Na^+ -ions [14]. For the alumina coated TiS_2 sample, the electrode needed to be equilibrated at different potentials for nearly 5 h. The potential value taken for this sample is the one observed after recording the impedance spectra. The R_{ct} values deduced from the impedance plot for alumina coated TiS_2 also suggest the increased impedance as the values obtained are three order magnitude higher than those obtained for uncoated samples. Interestingly, near the strong lithiation potential plateau at ~1.42 V the R_{ct} increases to be maximum with the order of 10^5 value (figure S7(b)). While observing the EIS plot for alumina coated sample, it is evident that even in lower frequency region a steady line is not observed instead a curved line suggesting deviation from normal diffusion behavior. To calculate the D_{Li+}, impedance data are selected of the potential at which characteristic linear Warburg diffusion is observed at lower frequency. The calculated values of D_{Li+} for alumina coated TiS_2 is lesser then that for Na^+ ion diffusion in bare TiS_2 sample. However, all these diffusion coefficients calculated (figure 8) in bare TiS_2 for Li^+ with $LiPF_6$ and Na^+ with $NaClO_4$, and in alumina coated TiS_2 with for Li^+ with $LiPF_6$ lies in the range as reported for the layered TiS_2 [5, 12]. The observed diffusion coefficient values are different from the values measured by Cottrell equation [32] ($D_{Li+} = 0.4$ to 4.0×10^{-9} and $D_{Na+} = 0.3$ to 3.2×10^{-9} cm^2 s^{-1}) in which the separation of chemical and charge diffusion coefficient is not feasible. However, observed trend in diffusion coefficient in present study is strongly alkali ion diffusion dependent.

4. Conclusion

In the present study we have used thin film TiS_2 electrode to investigate alkali ion (Li^+ and Na^+) intercalation/de-intercalation behavior. The films grown by an optimized ALD fabrication process on a suitable substrate are without any binder and carbon additives. Intercalation of Li^+ and Na^+ -ion are observed to be different which are clearly evident from the cyclic voltammetry measurements. The diffusion coefficient, calculated by GITT, is found to be same for Li^+ and Na^+ -ion in the TiS_2 structure. The impedance analysis at different discharge potentials reveal a strong dependence on the intercalating ion, Li^+ or Na^+ -ion and a correlation between R_{ct} values with discharge potential has been stablished. The diffusion coefficients calculated from Warburg impedance is maximum for Li^+-ion diffusion throughout the lithiated state of TiS_2. The TiS_2 coated with alumina results in a stable SEI formation. However, the Li^+-ion diffusion coefficient is significantly lower leading to lower 1st cycle specific capacity and large irreversible capacity loss.

Acknowledgments

FNS would like to acknowledge Department of Science and Technology, India for the DST INSPIRE Faculty Fellowship. AJB acknowledges the Amrut Mody Chair Professorship and DST-Nano Mission (DST/NM/NS/2018/257(G)) for financial support.

ORCID iDs

Farheen N Sayed https://orcid.org/000-0002-5700-5959
M B Sreedhara https://orcid.org/0000-0003-4925-4346
Ranjan Datta https://orcid.org/0000-0002-8553-3724
Aninda J Bhattacharyya https://orcid.org/0000-0002-0736-0004
C N R Rao https://orcid.org/0000-0003-4088-0615

References

[1] Kato K, Sayed F N, Babu G and Ajayan P M 2018 *2D Materials* **5** 025016
[2] Lin D, Liu Y, Liang Z, Lee H-W, Sun J, Wang H, Yan K, Xie J and Cui Y 2016 *Nature Nanotechnology* **11** 626
[3] Zhu K, Guo S, Yi J, Bai S, Wei Y, Chen G and Zhou H 2015 *J. Mater. Chem. A* **3** 22012
[4] Samad A, Shafique A and Shin Y-H 2017 *Nanotechnology* **28** 175401
[5] Van der Ven A, Bhattacharya J and Belak A A 2013 *Acc. Chem. Res.* **46** 1216
[6] Sun X, Bonnick P and Nazar L F 2016 Layered TiS_2 positive electrode for Mg batteries *ACS Energy Letters* **1** 297–301
[7] Suslov E A, Bushkova O V, Sherstobitova E A, Reznitskikh O G and Titov A N 2016 Lithium intercalation into TiS_2 cathode material: phase equilibria in a Li–TiS_2 system *Ionics* **22** 503–14
[8] Tchitchekova D S, Ponrouch A, Verrelli R, Broux T, Frontera C, Sorrentino A, Bardé F, Biskup N, Arroyo-de Dompablo M E and Palacín M R 2018 Electrochemical intercalation of calcium and magnesium in TiS_2: fundamental studies related to multivalent battery applications *Chemistry of Materials* **30** 847–56
[9] Wang L *et al* 2018 TiS_2 as a high performance potassium ion battery cathode in ether-based electrolyte *Energy Storage Materials* **12** 216–22
[10] Kasai H *et al* 2018 X-ray electron density investigation of chemical bonding in van der Waals materials *Nature Materials* **17** 249–52
[11] Whittingham M S 1976 Electrical energy storage and intercalation Chemistry *Science* **192** 1126
[12] Hawkins C G and Whittaker-Brooks L 2018 Vertically oriented TiS_{2-x} nanobelt arrays as binder- and carbon-free intercalation electrodes for Li- and Na-based energy storage devices *Journal of Materials Chemistry A* **6** 21949–60
[13] Tian B *et al* 2017 Phase transformations in TiS_2 during K intercalation *ACS Energy Letters* **2** 1835–40
[14] Whittingham M S 1978 Chemistry of intercalation compounds: metal guests in chalcogenide hosts *Progress in Solid State Chemistry* **12** 41–99
[15] Carmalt C J, Parkin I P and Peters E S 2003 Atmospheric pressure chemical vapour deposition of TiS_2 thin films on glass *Polyhedron* **22** 1263–9
[16] Chang H S W and Schleich D M 1992 TiS_2 and TiS_3 thin films prepared by MOCVD *Journal of Solid State Chemistry* **100** 62–70
[17] Matsuyama T, Sakuda A, Hayashi A, Togawa Y, Mori S and Tatsumisago M 2012 Preparation of amorphous TiSx thin film electrodes by the PLD method and their application to all-solid-state lithium secondary batteries *Journal of Materials Science* **47** 6601–6
[18] Zehnder D, Deshpandey C, Dunn B and Bunshah R F 1986 Transport properties of thin film TiS_2 produced by are *Solid State Ionics* **18-19** 813–7
[19] Mahuli N and Sarkar S K 2014 Atomic layer deposition of titanium sulfide and its application in extremely thin absorber solar cells *Journal of Vacuum Science & Technology A* **33** 01A150
[20] Pore V, Ritala M and Leskelä M 2007 Atomic layer deposition of titanium disulfide thin films *Chemical Vapor Deposition* **13** 163–8
[21] Weppner W and Huggins R A 1977 Determination of the kinetic parameters of mixed-conducting electrodes and application to the system Li_3Sb *Journal of The Electrochemical Society* **124** 1569–78
[22] Das S, Dutta D, Araujo R B, Chakraborty S, Ahuja R and Bhattacharyya A J 2016 Probing the pseudo-1-D ion diffusion in lithium titanium niobate anode for Li-ion battery *Physical Chemistry Chemical Physics* **18** 22323–30
[23] Li P, Zheng X, Yu H, Zhao G, Shu J, Xu X, Sun W and Dou S X 2019 Electrochemical potassium/lithium-ion intercalation into $TiSe_2$: kinetics and mechanism *Energy Storage Materials* **16** 512–8
[24] Verma A, Smith K, Santhanagopalan S, Abraham D, Yao K P and Mukherjee P P 2017 Galvanostatic intermittent titration and performance based analysis of $LiNi_{0.5}Co_{0.2}Mn_{0.3}O_2$ cathode *Journal of The Electrochemical Society* **164** A3380–92
[25] Ho C, Raistrick I D and Huggins R A 1980 Application of A-C techniques to the study of lithium diffusion in tungsten trioxide thin films *Journal of The Electrochemical Society* **127** 343–50
[26] Li W-D, Xu C-Y, Du Y, Fang H-T, Feng Y-J and Zhen L 2014 Electrochemical lithium insertion behavior of β-LixV_2O_5 ($0 < x \leqslant 3$) as the cathode material for secondary lithium batteries *Journal of The Electrochemical Society* **161** A75–83
[27] Abendroth R P 1957 *A Thermodynamic Study of the Titanium Sulfides.* (Michigan: University of Missouri, Ann Arbor) http://merlin.lib.umsystem.edu/record=b2610334~S8
[28] Sandoval S J, Chen X K and Irwin J C 1992 Raman spectra of Ag_xTiS_2 and lattice dynamics of TiS_2 *Physical Review B* **45** 14347–53
[29] Sreedhara M B, Gope S, Vishal B, Datta R, Bhattacharyya A J and Rao C N R 2018 Atomic layer deposition of crystalline epitaxial MoS_2 nanowall networks exhibiting superior performance in thin-film rechargeable Na-ion batteries *Journal of Materials Chemistry A* **6** 2302–10
[30] Chianelli R R, Scanlon J C and Rao B M L 1979 *In situ* studies of electrode reactions: the mechanism of lithium intercalation in TiS_2 *Journal of Solid State Chemistry* **29** 323–37
[31] Liu Y, Wang H, Cheng L, Han N, Zhao F, Li P, Jin C and Li Y 2016 TiS_2 nanoplates: a high-rate and stable electrode material for sodium ion batteries *Nano Energy* **20** 168–75
[32] Vaccaro A J, Palanisamy T, Kerr R L and Maloy J T 1982 Electrochemical investigations of alkali-metal intercalation reactions in TiS_2: chronoamperometric determination of mass and charge transport properties of liquid electrolyte systems *Journal of The Electrochemical Society* **129** 682–8